ACS OMEGA

http://pubs.acs.org/journal/acsodf

Article

1-Methyl-4-R-1,2,4-triazolium (R = $-CH_2CH_2OCH_3$, $-CH_2COOCH_2CH_3$)-Based Ionic Liquids as Plasticizers for Solid Propellants

Long Liu,* Jinhu Bai, Ze Su, Yuan Yao, Zhixiang Zhou, Yangfeng Xia,* and Yanqiang Zhang*

Cite This: *ACS Omega* 2023, 8, 16738−16747

Read Online

ACCESS | Metrics & More | Article Recommendations | Supporting Information

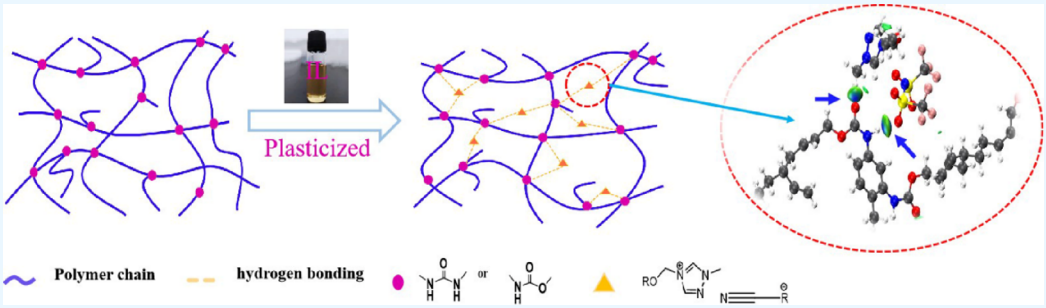

ABSTRACT: In this paper, a series of energetic ionic liquid plasticizers of 1-methyl-4-methoxyethyl-1,2,4-triazolium chloride (**1**), 1-methyl-4-methoxyethyl-1,2,4-triazolium bis(trifluoromethylsulfonyl)imide (**1a**), 1-methyl-4-methoxyethyl-1,2,4-triazolium nitrate (**1b**), 1-methyl-4-ethyl acetate-1,2,4-triazolium chloride (**2**), 1-methyl-4-ethyl acetate-1,2,4-triazolium bis(trifluoromethylsulfonyl)-imide (**2a**), and 1-methyl-4-ethyl acetate-1,2,4-triazolium nitrate (**2b**) were synthesized and characterized. The results show that compounds **1a**, **1b**, **2a**, and **2b** have lower melting points (T_m, −72.60 to −32.67 °C) and good thermal stability (T_d, 161−348 °C) and are suitable as plasticizers for hydroxyl-terminated polybutadiene (HTPB) curing systems. Among these four ionic liquids, ester-functionalized cations can help to improve the tensile strength (**2a**, 0.943 MPa; **2b**, 1.113 MPa) of the cured system, while ether-functionalized cations are more beneficial to improve elongation at break (**1a**, 522.90%; **1b**, 484.45%). Ester-functionalized ionic liquids are more beneficial to reduce the glass transition temperature of HTPB elastomers. The storage modulus of HTPB elastomers containing NO_3^- is higher, while that of HTPB elastomers containing NTf_2^- is lower. The crosslink densities of HTPB/TDI/**2a** and HTPB/TDI/**2b** plasticized by ester-functionalized ionic liquids are larger, which are 9369 and 9616 mol/m^3, respectively. There are hydrogen bond interactions between the ionic liquid and the HTPB elastomer, and these interactions changed the distribution of the hard and soft segments in the polymer molecules.

1. INTRODUCTION

Composite solid propellants are polymer-based composite energetic materials, which are an energy material for missiles, rockets, and other weapons or equipment. In addition to high combat performance, solid propellants must also meet certain environmental suitability and material processing performance, which requires solid propellants to meet certain mechanical properties.[1,2] Solid propellants are mainly composed of high-energy oxidants, metal fuels, binders, curing agents, plasticizers, etc. Among them, a plasticizer is an important mechanical property modifier. Adding a certain amount of plasticizer can make the polymer gel swell to promote molecular motion, improve processing performance and low-temperature mechanical properties, and then improve the low-temperature adaptability of solid propellants.[3] Plasticizers in hydroxyl-terminated polybutadiene (HTPB) solid propellants draw on many established plasticizers in the civilian industry, such as dioctyl sebacate (DOS), dioctyl adipate (DOA), dibutyl phthalate (DBP), and dioctyl phthalate (DOP). These plasticizers not only modified the mechanical properties but also greatly improved the processing properties of the propellant. However, these plasticizers do not contain energy, and adding too much will reduce the energetic properties of the solid propellant. On the other hand, these plasticizers will undergo molecular migration in the composite material system to form a significant slip layer, resulting in viscoplastic flow behavior, which will greatly affect the processability and plasticity of the propellant system.[4−7] Therefore, the selection and development of new energetic plasticizers are of great

Received: January 13, 2023
Accepted: March 27, 2023
Published: May 1, 2023

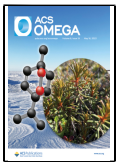

ACS Publications

© 2023 The Authors. Published by American Chemical Society

significance to further meet the requirements of new high energy solid propellants for low-temperature mechanical properties, high energy, and high reliability.

Room temperature ionic liquids (ILs) are low-temperature organic molten salts, which are usually liquid at around room temperature. ILs have the characteristics of good compatibility and thermal stability, wide liquid temperature range, strong polarity, etc. and can be structurally functionalized as needed, and they are often used as functional materials, green solvents, and catalysts.[8−10] ILs have a large number of hydrogen bonds and electrostatic interactions between anions and cations. When used as a polymer material additive, it can effectively inhibit molecular migration and improve mechanical properties, so ionic liquids have the potential as functional plasticizers.[11−15] For example, Zornio et al. used 1-butyl-3-methylimidazolium hexafluorophosphate ([C_4mim][PF_6]) as a plasticizer for polymethyl methacrylate (PMMA), and the results showed that ILs can be designed to have a wider range of mechanical properties than dioctyl phthalate (DOP);[16,17] Rahman and Brazel used IL with 1-butyl-3-methylimidazole as a cation to plasticize polyvinyl chloride (PVC), and the plasticized PVC showed good thermomechanical compatibility, migration, and leaching resistance;[18,19] Tang et al. also studied the plasticizing effect of ionic liquids on common nonpolar polymers polypropylene (PP) and polyethylene (PE).[20] It can be seen that ionic liquids have a good plasticizing effect on both polar and nonpolar polymers. Among so many ionic liquids, triazole and guanidine ionic liquids contain more N−N and C−N bonds and have higher enthalpy of formation, so they are also called energetic ionic liquids.[21−25] These ionic liquids have a good plasticizing effect on the adhesive system for solid propellants. Using these ionic liquids as plasticizers for solid propellants not only solves the problem of plasticizing solid propellants but also enables them to maintain high energy. This provides a new idea for the research of new energetic plasticizers, but there are relatively few studies on energetic ionic liquid plasticizers.

In this paper, we designed and synthesized a class of 1-methyl-4-R-1,2,4-triazolium-based ionic liquids (R = $-CH_2CH_2OCH_3$, $-CH_2COOCH_2CH_3$) by introducing functional groups of ether or esters into energetic triazole structures, which improves its plasticizing effect on solid propellant binders. The physical and chemical properties of the prepared ionic liquids were studied in detail, and the curing process of the HTPB/TDI/ILs curing system and the properties of the cured product were analyzed in depth. Finally, the curing reaction mechanism was analyzed by infrared spectroscopy and theoretical calculations.

2. EXPERIMENTAL SECTION

2.1. Materials. The materials used were silver nitrate (99%, 3A Chemistry), 1-methyl-1,2,4-triazole (98%, Macleans), ethyl chloroacetate (99%, Aladdin), chloroethyl methyl ether (98%, Aladdin), acetonitrile (99%, Tianjin Guangfu), tetrahydrofuran (99%, Tianjin Damao), ethyl acetate (99%, Beijing Chemical Industry), ethanol (99.7%, Tianjin Damao), methanol (99.7%, Tianjin Damao), hydroxyl-terminated polybutadiene (molecular weight: 2700−3300, 3A Chemistry), bis (2-ethylhexyl) adipate (98%, Aladdin), 2,4-toluene diisocyanate (98%, Tokyo Chemical Industry Co., Ltd.), and bis(trifluoro methylsulfonyl)imide lithium salt (97%, Mooney Chemical Technology Co., Ltd.).

2.2. Characterizations. ^{1}H NMR and ^{13}C NMR were obtained on a Bruker liquid nuclear magnetic resonance spectrometer with a magnetic field strength of 600 MHz. The infrared spectrum of the sample was tested using a Fourier transform infrared spectrometer (Nicolet380). The content of C, H, N, and S was tested using an elemental analyzer. The melting point was obtained from a Swiss Mettler-Toledo differential scanning calorimeter with a nitrogen flow rate of 50 mL/min and a heating rate of 10 °C/min. Thermal decomposition temperature was measured using a TA Instruments Thermogravimetric Differential Thermal Analysis (TG-DTA) instrument with a heating rate of 10 °C/min and a temperature range of 25−600 °C. Ae dynamic mechanical thermal analysis (DMTA, TA Q800) instrument was used to measure the glass transition temperature (T_g), the loss modulus (tan δ), and the storage modulus of the HTPB curing system network, and a fixed frequency of 1 Hz was used at a heating rate of 3 °C/min over a temperature range from −100 to 50 °C; the mechanical properties were investigated on a Shanghai Xieqiang CTM8050 electronic universal testing machine with a tensile rate of 2 mm/min, at least five dumbbell-shaped specimens were made for each sample, and the average value was taken as the result. The microstructure of the cured system was observed using an AFM (Bruker MultiMode 8, Germany), and the phase diagram was obtained in tapping mode; ESI-MS was tested using a Bruker LCMS/ESI/QTOF.

2.3. Synthesis of Ionic Liquids. *2.3.1. 1-Methyl-4-methoxyethyl-1,2,4-triazolium Chloride (**1**).* 1-Methyl-1,2,4-triazole (48.46 g, 0.58 mol) and chloroethyl methyl ether (68.214 g, 0.722 mol) were dissolved in 100 mL of ethyl acetate. The mixture was stirred at 100 °C for 48 h, and then, the solvent was evaporated and removed to give a yellow liquid of 1-methyl-4-methoxyethyl-1,2,4-triazolium chloride. (80.685 g, yield 77.88%). ^{1}H NMR (600 MHz, d_6-DMSO): δ = 10.72 (s, 1H, CH), 9.53 (s, 1H, CH), 4.59−4.52 (m, 2H, CH_2), 4.12 (s, 3H, CH_3), 3.78−3.69 (m, 2H, CH_2), 3.32−3.22 ppm (m, 3H, CH_3). ^{13}C NMR (151 MHz, d_6-DMSO): δ = 145.39, 143.62, 69.39, 58.53, 47.62, 39.08 ppm. IR(KBr): ν = 3141, 3077, 3002, 1747, 1583, 1350, 1232, 1169, 1076, 1021, 981, 829 cm^{-1}. Elemental analysis of $C_6H_{12}ClN_3O$ (%): C 40.57, H 6.81, N 23.66. Experimental values: C 39.39, H 7.35, N 23.57.

*2.3.2. 1-Methyl-4-ethylacetate-1,2,4-triazolium Chloride (**2**).* 1-Methyl-1,2,4-triazole (49.87 g, 0.60 mol) and ethyl chloroacetate (88.41 g, 0.72 mol) were dissolved in 100 mL of tetrahydrofuran to obtain a mixed solution, which was stirred at 90 °C for 48 h. The lower solvent was evaporated, and then, the residue was dissolved in 150 mL of acetonitrile, and it was placed in a refrigerator for 12 h to obtain a white precipitate, filtered, and dried to obtain 1-methyl-4-ethylacetate-1,2,4-triazolium chloride. (83.24 g, yield 67.5%). ^{1}H NMR (600 MHz, d_6-DMSO): δ = 10.33 (s, 1H, CH), 9.31 (s, 1H, CH), 5.45 (s, 2H, CH_2), 4.23 (q, 2H, CH_2), 4.16 (s, 3H, CH_3), 1.26 ppm (t, 3H, CH_3). ^{13}C NMR (151 MHz, d_6-DMSO): δ = 166.75, 145.91, 144.18, 62.64, 48.59, 14.43 ppm. IR(KBr): ν = 3057, 2970, 1740, 1580, 1537, 1433,1395, 1375, 1348, 1235, 1171, 1077, 1020, 978, 900, 871, 774, 718, 661, 628, 417, 409 cm^{-1}. Elemental analysis of $C_7H_{12}ClN_3O_2$(%): C 40.89, H 5.88, N 20.44; Experimental values: C 40.39, H 5.925, N 20.74.

*2.3.3. 1-Methyl-4-methoxyethyl-1,2,4-triazolium Bis-(trifluoromethylsulfonyl)imide (**1a**).* 1-Methyl-4-methoxyethyl-1,2,4-triazolium chloride (70.89 g, 0.39 mol) was dissolved in 100 mL of deionized water, and NTf_2Li (126.13 g, 0.43

https://doi.org/10.1021/acsomega.3c00256
ACS Omega 2023, 8, 16738−16747

Scheme 1. Synthesis of 1-Methyl-4-R-1,2,4-triazolium (R = $-CH_2CH_2OCH_3$, $-CH_2COOCH_2CH_3$)-Based Ionic Liquids

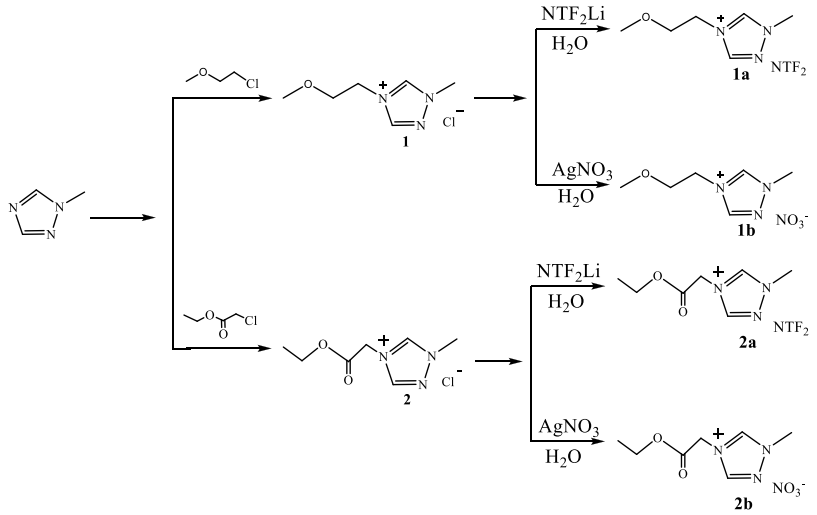

mol) was dissolved in 100 mL of deionized water; then, the two solutions were mixed and stirred at room temperature for 12 h, and the system was divided into two phases. The lower organic phase was washed several times with deionized water and then dissolved in methanol, dried by adding an appropriate amount of anhydrous magnesium sulfate, and the solution was placed at a low temperature overnight and filtered; the filtrate was evaporated to obtain a yellow liquid of 1-methyl-4-methoxylethyl-1,2,4-triazolium bis(trifluoromethylsulfonyl)-imide (105.91 g, yield 62.8%). ^{1}H NMR (600 MHz, d_6-DMSO): δ = 10.02 (s, 1H, CH), 9.14 (s, 1H, CH), 4.46−4.44 (m, 2H, CH_2), 4.08 (s, 3H, CH_3), 3.72−3.70 (m, 2H, CH_2), 3.30 ppm (s, 3H, CH_3). ^{13}C NMR (151 MHz, d_6-DMSO): δ = 166.6, 145.8, 144.1, 123.1, 121.0, 118.8, 116.7, 62.6, 48.5, 14.30 ppm. IR (KBr): ν = 3147, 1583, 1351, 1393, 1137, 1056, 1015, 790, 740, 664, 643, 617, 571, 514 cm^{-1}. Elemental analysis for $C_8H_{12}F_6N_4O_5S_2$(%): C 22.75, H 2.86, N 13.27, S 15.18; Experimental values: C 22.91, H 2.54, N 13.53, S 14.96.

*2.3.4. 1-Methyl-4-methoxyethyl-1,2,4-triazolium Nitrate (**1b**).* 1-Methyl-4-methoxyethyl-1,2,4- triazolium chloride (84.90 g, 0.47 mol) and silver nitrate (81.28 g, 0.47 mol) were dissolved in 100 mL of deionized water. The two solutions were then mixed and stirred at room temperature for 12 h to form a large white precipitate. After the white precipitate was removed by filtration, the filtrate was evaporated to dryness to obtain the crude product. After dissolving the crude product with excess acetonitrile, sodium chloride solution was added dropwise to remove excess silver nitrate, and the filtrate was evaporated to obtain the final product (73.01 g, yield 74.8%). ^{1}H NMR (600 MHz, d_6-DMSO): δ = 10.14 (s, 1H, CH), 9.20 (s, 1H, CH), 4.48−4.45 (m, 2H, CH_2), 4.10 (s, 3H, CH_3), 3.73−3.70 (m, 2H, CH_2), 3.29 ppm (s, 3H, CH_3). ^{13}C NMR (151 MHz, d_6-DMSO): δ = 145.3, 143.8, 69.3, 58.5, 47.5, 39.0 ppm. IR (KBr): ν = 3147, 1583, 1351, 1193, 1137, 1056, 1015, 790, 740, 664, 643, 617, 571, 514 cm^{-1}. Elemental analysis (%): $C_6H_{12}N_4O_4$: C 35.00, H 5.92, N 27.44. Experimental values: C 34.73, H 6.212, N 27.27.

*2.3.5. 1-Methyl-4-ethylacetate-1,2,4-triazolium bis-(trifluoromethylsulfonyl)imide (**2a**).* 1-Methyl-3-ethylacetate-1,2,4-triazolium chloride (78.24 g, 0.38 mol) and NTf_2Li (119.64 g, 0.42 mol) were dissolved in 100 mL of deionized water. The two obtained solutions were stirred at 25 °C for 12 h, and the reaction was divided into two phases. The lower organic phase was washed several times with deionized water and then dissolved in methanol and dried by adding an appropriate amount of anhydrous magnesium sulfate, and the solution was placed at a low temperature overnight and filtered; the filtrate was evaporated to obtain a colorless liquid of 1-methyl-4-ethylacetate-1,2,4-triazolium bis-(trifluoromethylsulfonyl)imide (148.21 g, yield: 86.4%). ^{1}H NMR (600 MHz, d_6-DMSO): δ = 10.04 (s, 1H, CH), 9.14 (s, 1H, CH), 5.32 (s, 2H, CH_2), 4.25 (q, 2H, CH_2), 4.14 (s, 3H, CH_3), 1.27 ppm (t, 3H, CH_3). ^{13}C NMR (151 MHz, d_6-DMSO): δ = 166.6, 145.8, 144.1, 123.1, 121.0, 118.8, 116.7, 62.6, 48.5, 14.3 ppm. IR(KBr): ν = 3150, 3103, 2991, 1753, 1586, 1439, 1350, 1194, 1136, 1056, 1020, 983, 790, 741, 656, 617, 571, 514 cm^{-1}. The theoretical values (%) of $C_9H_{12}F_6N_4O_6S_2$ are C 24.00, H 2.69, N 12.44, S 14.24. Experimental values: C 24.38, H 1.98, N 12.97, S 14.42.

*2.3.6. 1-Methyl-4-ethylacetate-1,2,4-triazolium Nitrate-(**2b**).* 1-Methyl-4-ethylacetyl-1,2,4- triazolium chloride (98.62 g. 0.48 mol) and silver nitrate (81.53 g, 0.48 mol) were dissolved in 100 mL of deionized water. The two obtained solutions were mixed and stirred at 25 °C for 12 h, and a large amount of white precipitate was formed. After filtering out the white precipitate, the filtrate was evaporated to obtain a yellow viscous crude product. The crude product was dissolved in methanol, and NaCl solution was added dropwise at 60 °C to remove excess silver nitrate. After filtration and evaporation, excess acetonitrile was added and dried with anhydrous magnesium sulfate. The filtrate was evaporated to obtain the final product (101.21 g, yield 90.8%). ^{1}H NMR (600 MHz, d_6-DMSO): δ = 10.14 (s, 1H, CH), 9.20 (s, 1H, CH), 4.48−4.45 (m, 2H, CH_2), 4.10 (s, 3H, CH_3), 3.73−3.70 (m, 2H, CH_2), 3.29 ppm (s, 3H, CH_3). ^{13}C NMR (151 MHz, d_6-DMSO): δ = 167.9, 145.9, 62.6, 48.6, 39.3, 14.4 ppm. IR(KBr): ν = 3078, 3002, 1749, 1583, 1375, 1234, 1188, 1169, 1076, 1021, 981 cm^{-1}. Elemental analysis (%): $C_7H_{12}N_4O_5$ Theoretical values: C 36.21, H 5.21, N 24.13. Experimental values: C 33.69, H 5.084, N 24.59.

2.4. Preparation of Thermoset Materials. The Teflon molds coated with silicone oil were preheated to 80 °C for further use. The optimum amounts of HTPB (89%), TDI (8%), and ionic liquid plasticizer (3%) were mixed in a flask and stirred at 50 °C until completely dissolved; meanwhile, the

https://doi.org/10.1021/acsomega.3c00256
ACS Omega 2023, 8, 16738−16747

flask was connected to the vacuum pump, and the bubbles in the mixture were removed by vacuuming during stirring. When the mixture became viscous, the mixture was poured into the preheated mold, the mold was put into a vacuum drying oven, and finally, the mixture was cured at 60 °C for 7 days according to the prescribed curing process.[26]

2.5. Simulation. First-principles calculations were employed to explore the interaction between HTPB/TDI and **1a** by using the Vienna ab-initio simulation package (VASP) based on density functional theory (DFT).[27,28] For structural optimization, a Perdew−Burke−Ernzerhof functional (GGA-PBE) was employed to calculate the exchange and correlation effects. The self-consistent accuracy was set to 10^{-5} eV, and the force convergence was set to 0.02 eV·Å^{-1}. Meanwhile, the plane wave energy cutoff was set as 400 eV. K-points were sampled in the Monkhorst−Pack grid for the first Brillouin zone integration.[29,30] Then, an independent gradient model (IGM) based on molecular density[31] was employed to analyze interaction in **1a**/HTPB/TDI via Multiwfn software.[32]

2.6. Atomic Force Microscopy Test. AFM phase diagrams were obtained with a Multimode 8 AFM unit equipped with a Nano-Scope V controller and Nano Scope version 1.8 software (Veeco/Digital Instruments, Santa Barbara, CA). The AFM was measured in tap mode to obtain the height and phase diagrams, which were analyzed and processed by Nano Scope version 1.8 software.

3. RESULTS AND DISCUSSION

3.1. Synthesis. As shown in Scheme 1, the products were synthesized according to a general formulation of quaternization and ion exchange. Compounds **1** and **2** were solid at room temperature, and the rest were liquid at room temperature. Details of the synthesis process are given in Section 2.3. The structures of all ionic liquids were characterized by ^{1}H and ^{13}C NMR and IR spectra, and their purity was tested by elemental analysis. In the ^{1}H NMR spectrum, the chemical shifts of the H atoms of C−H bonds in triazole were 9.14−10.78 ppm. In the ^{13}C NMR spectrum, the chemical shifts of the carbon atoms of NTf_2^- in **1a** and **2a** were near 116−123 ppm. In IR spectrum, the absorption band of NO_3^- was in the range of 1355 cm^{-1}.[33] The absorption band of the C−F bond in NTf_2^- is around 1350 cm^{-1}. Around 1580 cm^{-1} is the absorption of the stretching vibration of C═N, which decreases the electron cloud density and appears red-shifted due to the presence of conjugation effects.

3.2. Physicochemical Properties of Ionic Liquids. The melting point (T_m) and decomposition temperature (T_d) of the prepared ionic liquid plasticizers were measured by DSC and TGA, respectively, and the results are shown in Table 1. Due to the different structures of anions or cations, the corresponding ionic liquids have different melting points. For example, under the same cation of 1-methyl-4-methoxyethyl-1,2,4-triazolium, the melting points of the corresponding ionic liquids vary in the order of the following anions: Cl^- < NTf_2^- < NO_3^-. For the same cation of 1-methyl-3-ethylacetate-1,2,4-triazolium, the corresponding melting points change in the order of NTf_2^- < NO_3^- < Cl^-. The changes of these laws indicate that the different substituents of the cations have substantially changed the interaction force between the anions and the cations. Among these compounds, compounds **1** (T_m = 56.9 °C) and **2** (T_m = 113.58 °C) are solid at room temperature and are difficult to mix with the binder of HTPB, and they are not suitable for use as a plasticizer. The melting point of other compounds is in the range of −72.60 to −32.67 °C, which is more suitable for use as a plasticizer.

Table 1. ILs' Heat Flux and Viscosity Density

ILs	1	2	1a	2a	1b	2b
T_m (°C)[a]	56.9	113.5	−61.6	−72.6	−45.0	−32.6
T_d (°C)[b]	228.7	166.5	348.2	338.0	178.3	161.1
density (20 °C)/(g/cm^3)	1.38	1.41	1.52	1.55	1.29	1.36
viscosity (20 °C)/(mPa·s)			138	851	429	13,800

[a]Melting point. [b]Decomposition temperature.

In terms of thermal stability, these compounds remain stable up to 150 °C, with decomposition temperatures ranging from 161 to 348 °C. For the same cations, the decomposition temperature changes in the following order: NTf_2^- > Cl^- > NO_3^-.

3.3. Curing of Hydroxyl-Terminated Polybutadiene (HTPB) with Ionic Liquids. HTPB has been used as the main binder species in composite solid propellants since the 1860s.[34−37] HTPB is a polyhydroxy liquid prepolymer that is crosslinked with isocyanate to form polyurethane. Plasticizers are usually added during the reaction to lower the glass transition temperature and adjust the mechanical properties, which will keep the propellant elastic at lower temperatures without losing its physical properties.[34,38,39] To verify the plasticizing effect of ionic liquids, HTPB was selected as the binder system, toluene 2,6-diisocyanate (TDI) was used as the curing agent, and 3 wt % ionic liquid was added as the plasticizer. At the same time, dioctyl adipate (DOA), one of the most commonly used plasticizers in HTPB systems, was selected as a contrast plasticizer. The cured sample was obtained at 60 °C for 7 days. The cured samples were subjected to dynamic mechanical analysis and mechanical property testing, and the possible plasticization mechanism was explored by infrared spectroscopy and VASP simulation.

3.3.1. Mechanical Performance. As shown in Table 2, the mechanical properties of the HTPB curing system with ionic liquids as plasticizers were greatly improved. The tensile strength and elongation at break of the HTPB/TDI/DOA curing system were 0.619 MPa and 220.5%, respectively, while the tensile strengths of the HTPB/TDI/ILs curing system were in the range of 0.683−1.113 MPa, and the elongations at break ranged from 413 to 522%. The tensile modulus of the HTPB/TDI/ILs curing system is in the range of 0.486−0.760 MPa, and these values are higher than the 0.322 MPa of the HTPB/TDI/DOA curing system. For different ionic liquid plasticizers, the effect of cations on mechanical properties is more significant. Ester-functionalized cations (**2a**, 0.943 MPa; **2b**, 1.113 MPa) can help to improve the tensile strength of the cured system, while ether-functionalized cations (**1a**, 522.90%; **1b**, 484.45%) are more beneficial to improve elongation at break.

3.3.2. Dynamic Mechanical Thermal Analysis. The thermodynamic properties of HTPB-cured elastomers were analyzed using DMTA. Figure 1a shows the glass transition temperature of each sample, and the glass transition temperature of the HTPB/TDI/DOA curing system is −63.16 °C. After replacing DOA with an equivalent amount of ionic liquid, the glass transition temperature is at the range of −64.99 to

https://doi.org/10.1021/acsomega.3c00256
ACS Omega 2023, 8, 16738−16747

Table 2. Thermodynamic and Mechanical Properties of HTPB Elastomers

composition acronym	tan δ[a]	T_g (°C)[b]	E (MPa)[c]	ν_e (mol/m^3)[d]	σ_t (MPa)[e]	E_t (MPa)[f]	ε_t (%)[g]
DOA	1.446	−63.14	45.2	7555	0.619	0.32	220.5
1a	1.436	−63.62	24.4	4090	0.683	0.612	522.9
1b	1.312	−63.95	36.3	6094	0.794	0.72	484.4
2a	1.533	−64.16	55.8	9369	0.943	0.48	413.6
2b	1.575	−64.99	57.1	9616	1.113	0.76	434.8

[a]Loss modulus. [b]Glass transition temperature. [c]Storage modulus. [d]Cross-link density. [e]Tensile strength. [f]Tensile modulus. [g]Elongation at the break.

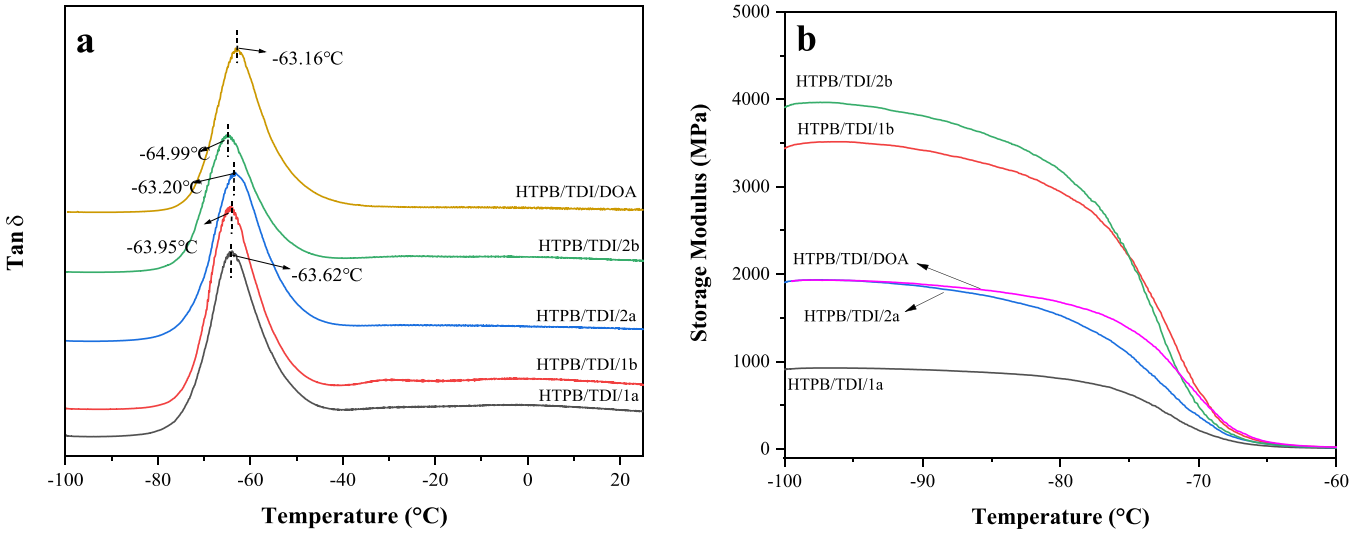

Figure 1. Dynamic mechanical thermal analysis curve of HTPB curing system. (a) Loss modulus (tan δ). (b) Storage modulus (E').

−63.20 °C, in which the glass transition temperature of HTPB plasticized by ester-functionalized ionic liquid decreased by 1.02 °C (**2a**) and 1.82 °C (**2b**). As can be seen from Figure 1b, when the temperature is lower than the glass transition temperature, the curing system is in a glass state, and HTPB/TDI/**2b** and HTPB/TDI/**1b** have higher storage modulus, which is much larger than that of the HTPB/TDI/DOA system; the storage modulus of the HTPB/TDI/**1a** system is much smaller than that of the HTPB/TDI/DOA system. The storage modulus of the HTPB/TDI/**2a** system is comparable to that of the HTPB/TDI/DOA system below −85 °C, but the decrease of the HTPB/TDI/**2a** system is larger than that of the HTPB/TDI/DOA system with an increase in temperature. The above results show that the anion of ionic liquid has a great influence on the storage modulus of the curing system. For the HTPB/TDI/ILs curing system, the storage modulus with the NO_3^- anion is higher, and the storage modulus with the NTf_2^- anion is lower. The above results show that the low-temperature elastic properties of the HTPB system plasticized by NTF_2^- ionic liquid are significantly improved, and the plasticizing performance is better than DOA.

The crosslink density of thermosets is related to their glass transition temperature and tan δ. The crosslink density of thermosets can be determined by eq 1[40]

$$\nu_e = \frac{E_r}{3RT_r} \quad (1)$$

where E_r is the storage modulus at the "rubber" state, $T_r = T_g + 30$, and ν_e is the crosslink density (mol/m^3).

As shown in Table 2, the cation of the ionic liquid has a greater effect on the crosslink density. The crosslink densities of the HTPB/TDI/**1a** and HTPB/TDI/**1b** curing systems with ether-functionalized ionic liquids as a plasticizer are 4090 and 6094 mol/m^3, respectively, which are smaller than those of the HTPB/TDI/DOA (7555 mol/m^3) curing system. The crosslink densities of HTPB/TDI/**2a** and HTPB/TDI/**2b** plasticized by ester-functionalized ionic liquids are larger, which are 9369 and 9616 mol/m^3, respectively. These results show that the interaction between the ester-functionalized cation and the HTPB system is stronger, and the tensile properties of the cured product are better, while the interaction between the ether-functionalized cation and the HTPB system is weaker, and the tensile strength of the cured product is weaker; these results are consistent with the results obtained from the tensile test.

3.3.3. Thermal Stability of Thermosets. The thermal stability of HTPB elastomers was studied using decomposition temperatures with 5 and 10% weight loss and the peak temperature of derivative thermogravimetry; the results are shown in Table 3.

When 3 wt % ionic liquid was added as a plasticizer, the decomposition temperature of the curing system decreased to a certain extent. The decomposition temperature corresponding to the first 5% weight loss was consistent with the decomposition temperature of ionic liquid. The variation of decomposition temperature of the HTPB/TDI/ILs system is consistent with that of ILs. When ionic liquids (**1a** and **2a**) with the NTf_2^- anion were used as plasticizers, it has a higher heat resistance ($T_{d\ 5\%}$ > 295 °C), and its heat resistance is better than that of the HTPB/TDI/DOA curing system ($T_{d\ 5\%}$ = 284.1 °C). The HTPB/TDI/**1a** curing system has the best heat resistance, and its $T_{d\ 10\%}$ and T_{max} values are 367.4 and

https://doi.org/10.1021/acsomega.3c00256
ACS Omega 2023, 8, 16738−16747

Table 3. Decomposition Temperatures of HTPB Elastomers

composition acronym	$T_{d\ 5\%}$ (°C)[a]	$T_{d\ 10\%}$ (°C)[b]	T_{max} (°C)[c]
HTPB/TDI	313.5	353.8	488.1
HTPB/TDI/DOA	284.1	337.7	448.4
HTPB/TDI/**1a**	309.9	367.4	504.3
HTPB/TDI/**2a**	295.9	354.0	484.5
HTPB/TDI/**1b**	258.1	323.5	486.2
HTPB/TDI/**2b**	288.2	342.7	485.1

[a]Decomposition temperature at 5% weight loss. [b]Decomposition temperature at 10% weight loss. [c]Peak temperature by a differential thermogravimetric method.

504.3 °C, respectively, which are even higher than those of the HTPB/TDI system ($T_{d\ 10\%}$ = 353.8 °C and T_{max} = 488.1 °C).

3.3.4. Infrared Spectrum Analysis of the HTPB/TDI/ILs System. The results of DMTA have shown that HTPB/TDI/**1a** and HTPB/TDI/**2a** systems exhibit a good low-temperature elasticity and plasticizing effect. To study the role of ionic liquids in the HTPB/TDI/ILs curing system, the variation of the absorption peaks of the main functional groups in the HTPB/TDI/**1a** and HTPB/TDI/**2a** systems was studied by FT-IR. The results are shown in Figure 2, Figure 3, and Figure 4.

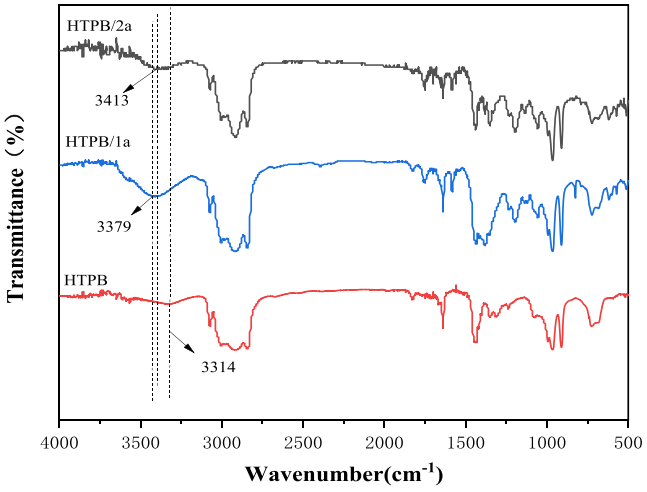

Figure 2. IR spectrum of the interaction between ILs and HTPB.

As shown in Figure 2, 3314 cm^{-1} is the absorption peak of −OH in HTPB, which red-shifts to 3379 and 3413 cm^{-1} with the addition of **1a** and **2a**, respectively. This indicates that a hydrogen bond is formed between the ionic liquids and the −OH groups in HTPB, thus extending the −OH bond and causing a red shift. When the ionic liquid is mixed with HTPB, molecules of the ionic liquid plasticizer will enter the gaps between the macromolecular chains of HTPB, destroy the hydrogen bond between the HTPB molecules, and then increase the distance between the HTPB molecules, thereby realizing the plasticization of HTPB.

Figure 3 shows the infrared spectra of the HTPB/TDI/**1a** system at different curing stages, and the main effect of the hydrogen bond in the infrared spectrum is to broaden the peaks.[40] As the reaction progressed, the −OH absorption peak around 3423 cm^{-1} gradually weakened, and a new absorption peak generated around 3350 cm^{-1} and then shifted to the right to 3330 cm^{-1} is the N−H stretching vibration in the carbamate, which was produced from the reaction of the hydroxyl group with the isocyanate.[41] According to the infrared spectrum in Figure 3, it can be seen that with the progress of the reaction, the peak position and intensity of the C═O bond in the urethane bond at 1640 cm^{-1} remain unchanged. The peak around 1530 cm^{-1} is the bending vibration peak of the N−H bond, the intensity of which increases with the reaction and shifts to the left to 1522 cm^{-1}[41]. The absorption peak at 1130 cm^{-1} is the symmetric stretching vibration peak of S═O in the ionic liquid, and the peak shape broadens with prolonged reaction, which may be caused by the formation of hydrogen bonds between S═O and N−H.

Figure 4 shows the infrared spectra of HTPB/TDI/**1a** and HTPB/TDI/**2a** systems after curing for 7 days. The peak at the 3349 cm^{-1} position is from the N−H bond stretching vibration in the urethane bond in HTPB/TDI. After adding ionic liquids as a plasticizer, the N−H stretching frequency decreases, and the peak shape widens and shifts to the lower wavenumber direction, with HTPB/TDI/**1a** peaking at 3324 cm^{-1} and HTPB/TDI/**2a** peaking at 3345 cm^{-1}. 1640 cm^{-1} is the peak of the C═O stretching vibration in the urethane bond, and 1531 cm^{-1} is the peak of the N−H bond deformation vibration. We can see from Figure 4 that the addition of the ionic liquid as a plasticizer increases the frequency of the N−H vibration and shifts it to the right to 1528 cm^{-1}, which proves that it is influenced by the hydrogen bond effect. The addition of a small amount of ionic liquid to the polymer matrix resulted in a peak at 1053 cm^{-1}, which is the peak of the S═O bond in the sulfone, demonstrating the presence of hydrogen bond between NTf_2^- and the carbamate bond.

3.3.5. Simulation of the HTPB/TDI/ILs System. The above research shows that the HTPB/TDI/**1a** curing system has the largest elongation at break (522.9%), the lowest low temperature storage modulus (<1000 MPa at <−80 °C), and the best thermal stability (T_{max} = 504.3 °C), indicating that **1a** has the best plasticizing effect on the HTPB/TDI system. To study the interaction between HTPB/TDI and **1a**, IGM calculations were employed by using Multiwfn.[32] As shown in Figure 5a, the value of δg can measure the interaction between fragments: the larger the value, the stronger the interaction. Also, there is a peak at the position of sign(λ_2) ρ = −0.02 to −0.03 a.u., where the electron density is relatively less. This indicates that strong interaction (nonchemical bond interaction) exists between HTPB/TDI and **1a**.[31] Then, the corresponding IGM three-dimensional spatial distribution map is shown in Figure 5b, where the color range is the same as Figure 5a. The results show that strong interactions are present in the blue space (space marked by arrows) corresponding to the hydrogen bond of −C−H...O with a bond length of 2.12 Å and a bond angle of 162.5° and the hydrogen bond of −N−H...O with a bond length of 2.01 Å and a bond angle of 169.5°. Therefore, a strong hydrogen bond interaction was formed between HTPB/TDI and **1a**, which makes the ionic liquid immobilized between molecular chains and effectively inhibits its molecular migration.

3.3.6. Microstructural Analysis. The HTPB/TDI/**1a** curing system showed the best mechanical properties and thermal stability. To study its microstructure, the AFM phase diagrams (Figure 6) of HTPB/TDI, HTPB/TDI/DOA, and HTPB/TDI/**1a** curing systems were obtained with a Multimode 8 AFM unit equipped with a Nano-Scope V controller and Nano Scope version 1.8 software. Figure 6a shows that the HTPB/

https://doi.org/10.1021/acsomega.3c00256
ACS Omega 2023, 8, 16738−16747

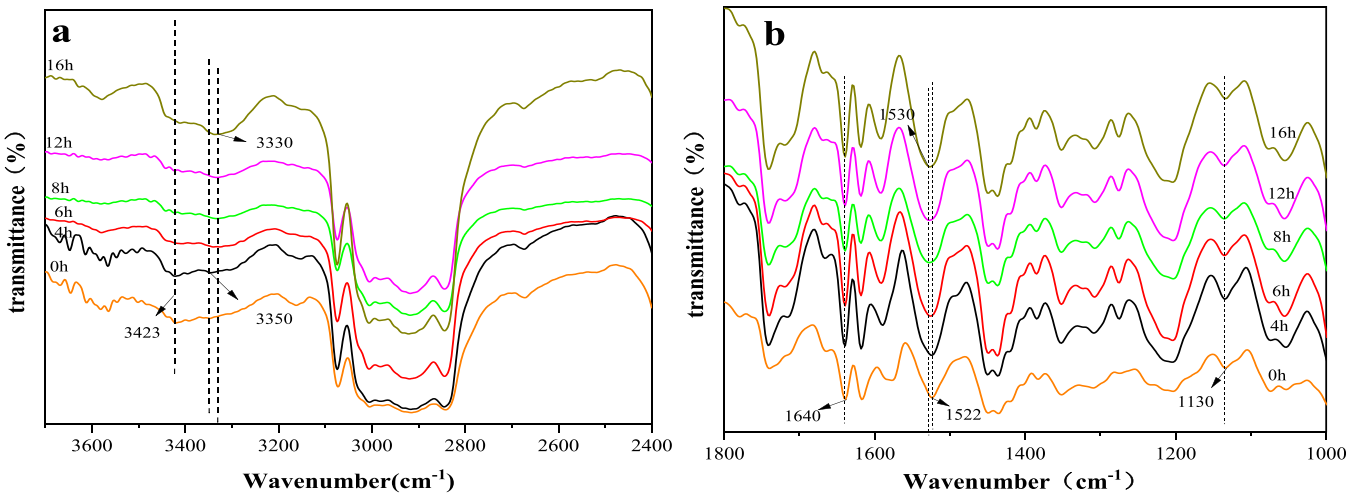

Figure 3. FT-IR spectra of HTPB/TDI/**1a** with different curing times. (a) Wavelength range 2400−3600 cm^{-1}. (b) Wavelength range 1000−1800 cm^{-1}.

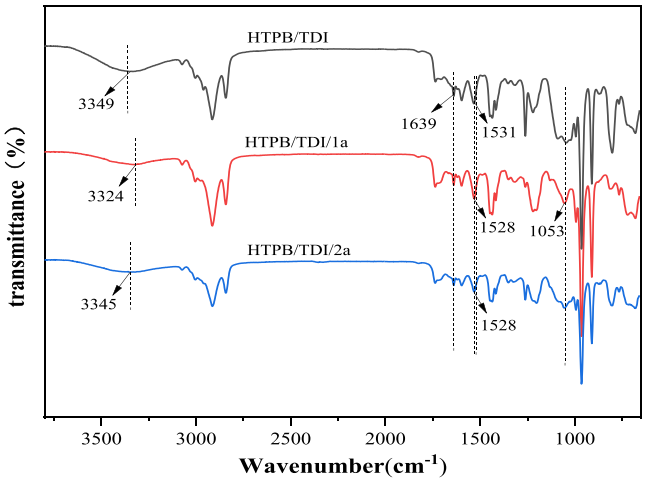

Figure 4. IR spectrum of the HTPB/TDI/IL system after curing for 7 days.

TDI curing system appears to have two bright and dark phases, indicating that phase separation does occur in the formed polymer.[42−44] This is due to the difference in cohesive energy density in the polyurethane polymer formed by the curing of the HTPB/TDI system, in which more polar urethane groups and urea bonds in the hard segment aggregate to form a brighter area, and the less polar carbon chains and C═C double bonds form darker regions in the soft segment aggregates.[45] When no plasticizer is added, there are fewer bright spots formed by HTPB/TDI curing in Figure 6a, indicating that the formed polyurethane polymer is dominated by soft segments and less hard segments are formed, in which a segment of polyurethane chain can be clearly seen. This is because the repeating unit of HTPB is a CH structure, which cannot form a hydrogen bond with the urethane of the hard segment, and the intermolecular force of the polymer is weak, and the resulting polyurethane cured product has low mechanical properties.

Figure 6b shows the AFM image of the HTPB/TDI/DOA curing system. The distribution area of bright spots is larger than that of the HTPB/TDI curing system, and the polyurethane segments are vaguely visible. This is because the −CO functional group in the DOA molecule forms a hydrogen bond with the −NH in the carbamate, which increases the force between the polyurethane hard segment chains to a certain extent, the bright spot area in the AFM diagram was increased, and the tensile strength was improved.

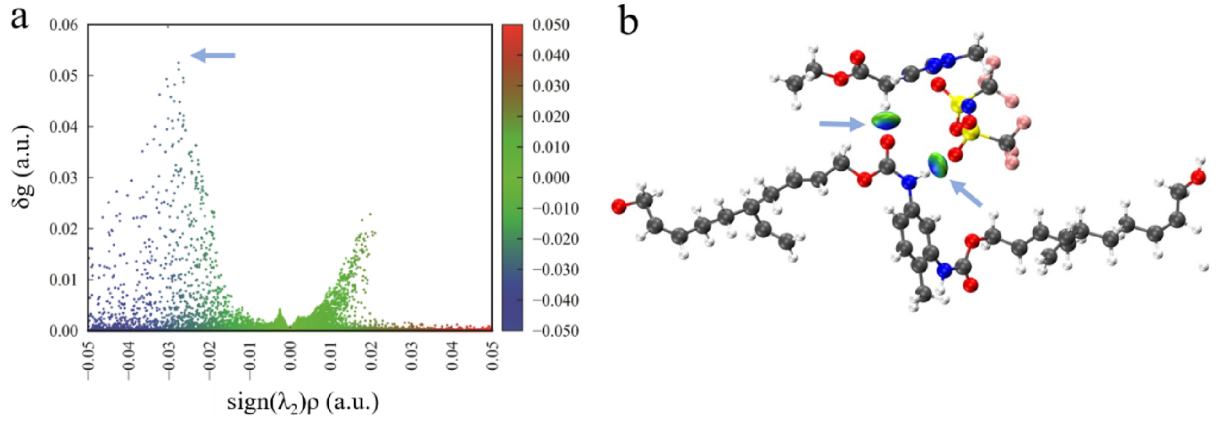

Figure 5. Independent gradient model (IGM). (a) Scattered points plot and (b) corresponding three-dimensional spatial distribution map (isosurface = 0.01 a.u.) of the HTPB/TDI/**1a** (the blue arrows represent the corresponding space in panel (a)).

https://doi.org/10.1021/acsomega.3c00256
ACS Omega 2023, 8, 16738−16747

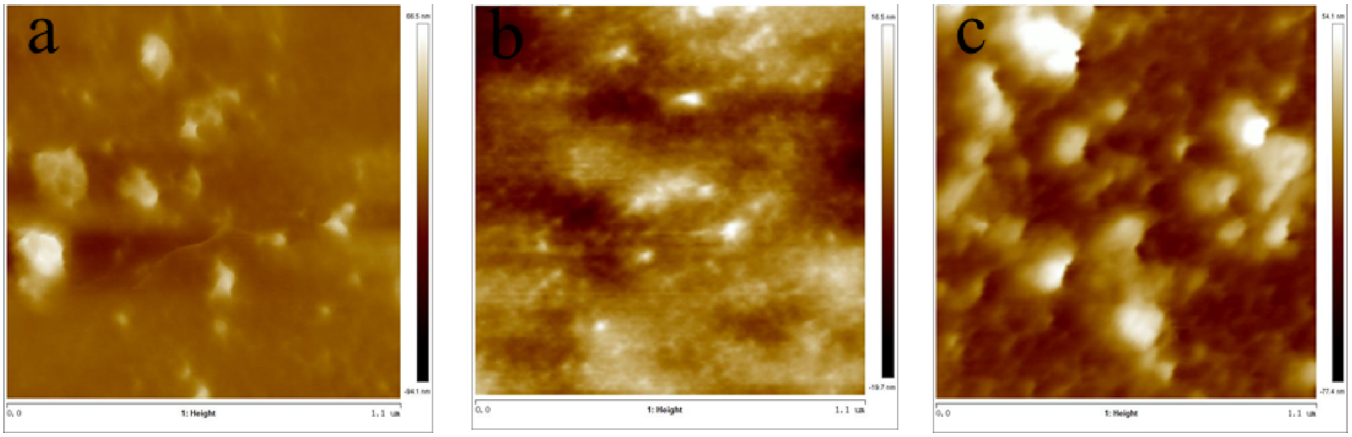

Figure 6. AFM phase diagrams of HTPB/TDI, HTPB/TDI/DOA, and HTPB/TDI/**1a**, observation size: 1.1 × 1.1 μm. (a) HTPB/TDI; (b)HTPB/TDI/DOA; (c) HTPB/TDI/**1a**.

Figure 6c shows the AFM image of the HTPB/TDI/**1a** curing system. When **1a** is used as the plasticizer, the area of the bright spot in the AFM image increases significantly, indicating that a large number of clusters are formed. This is because the anions and cations in **1a** form hydrogen bonds with the polyurethane segments. These hydrogen bonds cause the hard segments of the polymer to aggregate and bend to form clusters. The hard segment clusters improve the tensile strength of the polymer, and the bending of the segment also increases its elongation at break.

4. CONCLUSIONS

In summary, a series of new energetic ionic liquid plasticizers with 1-methyl-4-methoxyethyl-1,2,4-triazolium and 1-methyl-4-ethyl acetate-1,2,4-triazolium as cations were synthesized. Their performances under different anions of Cl^-, NTf_2^-, and NO_3^- were studied. The results show that compounds 1-methyl-4-methoxyethyl-1,2,4-triazolium bis-(trifluoromethylsulfonyl)imide (**1a**), 1-methyl-4-methoxyethyl-1,2,4-triazolium nitrate (**1b**), 1-methyl-4-ethyl acetate-1,2,4-triazolium bis(trifluoromethyl)sulfonimide (**2a**), and 1-methyl-4-ethyl acetate-1,2,4-triazolium nitrate (**2b**) have lower melting points (T_m, −72.60 to −32.67 °C) and better thermal stability (T_d, 161−348 °C) and are suitable as plasticizers for HTPB. Among these four ionic liquids, ester-functionalized cations can help to improve the tensile strength (**2a**, 0.943 MPa; **2b**, 1.113 MPa) of the cured system, while ether-functionalized cations are more beneficial to improve elongation at break (**1a**, 522.90%; **1b**, 484.45%). Ester-based ionic liquids are more conducive to reducing the glass transition temperature of HTPB elastomers. The anion of ionic liquid has a great influence on the storage modulus of the curing system: the storage modulus of HTPB elastomers containing NO_3^- anions is higher, while that of HTPB elastomers containing NTf_2^- anions is lower. The crosslink densities of HTPB/TDI/**2a** and HTPB/TDI/**2b** plasticized by ester-functionalized ionic liquids are larger, which are 9369 and 9616 mol/m^3, respectively. The HTPB/TDI/**1a** curing system has the largest elongation at break (522.9%), the lowest low temperature storage modulus (<1000 MPa at <−80 °C), and the best thermal stability (T_{max} = 504.3 °C), indicating that **1a** has the best plasticizing effect on the HTPB/TDI system. Infrared spectroscopy, AFM, and theoretical calculations show that there are hydrogen bond interactions between **1a** and the HTPB elastomer, and these interactions change the distribution of hard and soft segments in polymer molecules and improve the mechanical properties of the cured products. This study will provide theoretical and experimental guidance for the design of new plasticizers for HTPB binder systems.

■ ASSOCIATED CONTENT

Supporting Information

The Supporting Information is available free of charge at https://pubs.acs.org/doi/10.1021/acsomega.3c00256.

(Figure S1) ^{1}H NMR and ^{13}C NMR of the synthesized ionic liquids; (Figure S2) ionic liquid ESI diagram; (Figure S3) IR of the synthesized ionic liquids; (Figure S4) density viscosity of the synthesized ionic liquids; (Figure S5) ionic liquid TG graph; (Figure S6) loss modulus (E'') of thermosets; and (Figure S7) HTPB/TDI/IL tensile properties (PDF)

■ AUTHOR INFORMATION

Corresponding Authors

Long Liu − *Key Laboratory of Science and Technology on Particle Materials, Beijing Key Laboratory of Ionic Liquids Clean Process, Institute of Process Engineering, Chinese Academy of Sciences, Beijing 100049, China;* orcid.org/0000-0003-0681-1202; Email: lliu@ipe.ac.cn

Yangfeng Xia − *Institute of Systems Engineering, Academy of Military Science, Beijing 100071, China;* orcid.org/0000-0003-1476-3845; Email: xiayangfeng17@mails.ucas.edu.cn

Yanqiang Zhang − *Key Laboratory of Science and Technology on Particle Materials, Beijing Key Laboratory of Ionic Liquids Clean Process, Institute of Process Engineering, Chinese Academy of Sciences, Beijing 100049, China; Zhengzhou Institute of Emerging Industrial Technology, Zhengzhou 450000, China;* orcid.org/0000-0001-5577-0529; Email: yqzhang@ipe.ac.cn

Authors

Jinhu Bai − *Key Laboratory of Science and Technology on Particle Materials, Beijing Key Laboratory of Ionic Liquids Clean Process, Institute of Process Engineering, Chinese Academy of Sciences, Beijing 100049, China*

Ze Su − *Zhengzhou Institute of Emerging Industrial Technology, Zhengzhou 450000, China; Institute of*

https://doi.org/10.1021/acsomega.3c00256
ACS Omega 2023, 8, 16738−16747

Advanced Technology, Zhengzhou University, Zhengzhou 450002, China

Yuan Yao − *Zhengzhou Institute of Emerging Industrial Technology, Zhengzhou 450000, China*

Zhixiang Zhou − *Zhengzhou Institute of Emerging Industrial Technology, Zhengzhou 450000, China; Institute of Advanced Technology, Zhengzhou University, Zhengzhou 450002, China*

Complete contact information is available at: https://pubs.acs.org/10.1021/acsomega.3c00256

Author Contributions

The manuscript was written through contributions of all authors. All authors have given approval to the final version of the manuscript. L.L.: Made the experimental plan, wrote and modified the article; J.B.: Synthesized and characterized the compounds, wrote the draft; Z.S.: Processed the data and modified the article; Z.Z.: Performed the curing performance test; Y.Y.: Performed the theoretical calculation; Y.X.: Performed the theoretical calculation, data processing, and article modification; Y.Z.: Performed the experimental scheme formulation, experimental guidance, and article revision.

Notes

The authors declare no competing financial interest.

■ ACKNOWLEDGMENTS

This work was supported by the National Natural Science Foundation of China (22008245, 21878278, and U21A20307); Joint Fund of the Equipment Pre-Research of Chinese Academy of Sciences (8091A160104); Fundamental Strengthening Program Technology Field Fund (2021-JCJQ-JJ-1317); and National Defense Basic Research Project (JCKY2019130D006).

■ REFERENCES

(1) Pang, A. M. *Solid Rocket Propellant Theory and Engineering*. China, 2014.

(2) Beckstead, M. W.; Puduppakkam, K.; Thaker, P.; Yang, V. Modeling of Combustion and Ignition of Solid-propellant Ingredients. *Prog. Energ. Combust. Sci.* **2007**, *33*, 497−551.

(3) Min, B. *Design of Solid Rocket Motors for Air Defense Missiles*. China, 1993.

(4) He, J.; Lee, S. S.; Kalyon, D. M. Shear Viscosity and Wall Slip Behavior of Dense Suspensions of Polydisperse Particles. *J. Rheol. (N.Y.)*. **2019**, *63*, 19−32.

(5) Kalyon, D. M. Apparent Slip and Viscoplasticity of Concentrated Suspensions. *J. Rheol. (N.Y.)*. **2005**, *49*, 621−640.

(6) Kalyon, D. M.; Akta, S. S. Factors Affecting the Rheology and Processability of Highly Filled Suspensions. *Annu. Rev. Chem. Biomol. Eng.* **2014**, *5*, 229−254.

(7) Singh, A.; Radhakrishnan, S.; Vijayalakshmi, R.; Talawar, M. B.; Kumar, A.; Kumar, D. Screening of Polymer-plasticizer Systems for Propellant Binder Applications: An Experimental and Simulation Approach. *J. Energ. Mater.* **2019**, *37*, 1−13.

(8) Marsh, K. N.; Boxall, J. A.; Llchtenthaler, R. Room Temperature Ionic Liquids and Their Mixtures—A Review. *Fluid Phase Equilib.* **2004**, *219*, 93−98.

(9) Li, Z. M.; Zhong, Y. L.; Liang, N. Y.; Feng, G.; Zhang, J. G.; Zhang, T. L.; Zhang, Y. Q. Hypergolic Coordination Compounds as Modifiers for Ionic Liquid Propulsion. *Chem. Eng. J.* **2021**, *423*, 130187−130194.

(10) Xiang, S. F.; He, X. J.; Zheng, F.; Lu, Q. H. Multifunctional Flexible Sensors Based on Ionogel Composed Entirely of Ionic Liquid with Long Alkyl Chains for Enhancing Mechanical Properties. *Chem. Eng. J.* **2022**, *439*, 135644−135653.

(11) Chen, P.; Xie, F.; Tang, F.; Mcnally, T. Ionic Liquid (1-Ethyl-3-Methylimidazolium acetate) Plasticization of Chitosan-based Bionanocomposites. *ACS Omega* **2020**, *5*, 19070−19081.

(12) Clavero, E.; Rodriguez, J. Ionic Liquids at the Air/Water Interface. *J. Mol. Liq.* **2011**, *163*, 64−69.

(13) Li, Z. X.; Liu, N.; Yao, Y. B.; Chen, S. Y.; Wang, H. F.; Wang, H. P. Thermal Behavior of Cellulose Diacetate Melt Using Ionic Liquids as Plasticizers. *RSC Adv.* **2015**, *5*, 901−907.

(14) Singh, R. P.; Verma, R. D.; Meshri, D. T.; Shreeve, J. M. Energetic Nitrogen-rich Salts and Ionic Liquids. *Angew. Chem., Int. Ed.* **2006**, *37*, 3584−3601.

(15) Wang, H.; Gurau, G.; Rogers, R. D. Ionic Liquid Processing of Cellulose. *Chem. Soc. Rev.* **2012**, *41*, 1519−1537.

(16) Scott, M. P.; Brazel, C. S.; Benton, M. G.; Mays, J. W.; Holbrey, J. D.; Rogers, R. D. Application of Ionic Liquids as Plasticizers for Poly(methyl methacrylate). *Chem. Commun.* **2002**, *13*, 1370−1381.

(17) Zornio, C. F.; Livi, S.; Duchet-rumeau, J.; Gerard, J. F. Ionic Liquid-Nanostructured Poly(methyl methacrylate). *Nanomaterials* **2019**, *9*, 1376−1392.

(18) Rahman, M.; Brazel, C. S. Ionic Liquids: New Generation Stable Plasticizers for Poly (vinyl chloride). *Polym. Degrad. Stab.* **2006**, *91*, 3371−3382.

(19) Liu, D.; Shen, Y. R.; Jiang, P. P.; Wai, P. T.; Zhang, Z. M.; Zhang, P. B.; Agus, H. Y.; Nie, Z. X.; Zhao, M. Z.; Zhao, H. H. An Efficient Cold-Resistant Strategy: Synthesis and Application of Green Cold-resistant Bio-based Plasticizer for Poly(vinyl chloride). *Eur. Polym. J.* **2021**, *142*, 110154−110166.

(20) Tang, H. O.; Ding, Y. S.; Li, B. X. Effect of Imidazolium-based Ionic Liquid Br[C_{14}Im](CH_2)$_4$[C_{14}Im]Br on the Structure and Properties of PP. *J. Polym. Sci.* **2009**, *02*, 191−194.

(21) Zhang, Y. Q.; Parrish, D. A.; Shreeve, J. M. Derivatives of 5-Nitro-1,2,3-2H-triazole − High Performance Energetic Materials. *J. Mater. Chem. A* **2013**, *1*, 585−593.

(22) Xue, H.; Shreeve, J. M. Energetic Ionic Liquids from Azido Derivatives of 1,2,4-Triazole. *Adv. Mater.* **2005**, *17*, 2142−2146.

(23) Xue, H.; Twamley, B.; Shreeve, J. M. Energetic Salts of Substituted 1,2,4-Triazolium and Tetrazolium 3,5-Dinitro-1,2,4-triazolates. *J. Mater. Chem.* **2005**, *15*, 1731−1739.

(24) Jiang, Z. Y.; Wang, Q.; Liu, L.; Zhang, Y. Q.; Du, F.; Pang, A. M. Dual-functionalized Imidazolium Ionic Liquids as Curing Agents for Epoxy Resins. *Ind. Eng. Chem. Res.* **2020**, *59*, 3024−3034.

(25) Liu, L.; Gao, S.; Jiang, Z. Y.; Zhang, Y. Q.; Gui, D. Y.; Zhang, S. J. Amide-Functionalized Ionic Liquids as Curing Agents for Epoxy Resin: Preparation, Characterization, and Curing Behaviors with TDE-85. *Ind. Eng. Chem. Res.* **2019**, *58*, 14088−14097.

(26) Wu, X. Y.; Cui, Q. Z.; Xu, J. Curing Reaction Kinetics of HTPB/TDI Bonding System. *Ener. Mater.* **2016**, *24*, 1097−1101.

(27) Kresse, G.; Furthmuller, J. Efficient Iterative Schemes for Ab Initio Total-energy Calculations Using a Plane-wave Basis Set. *Phys. Rev. B* **1996**, *54*, 11169−11186.

(28) Kresse, G.; Furthmuller, J. Efficiency of Ab-initio Total Energy Calculations for Metals and Semiconductors Using a Plane-wave Basis Set. *Comput. Mater. Sci.* **1996**, *6*, 15−50.

(29) Perdew, J. P.; Burke, K.; Ernzerhof, M. Generalized Gradient Approximation Made Simple. *Phys. Rev. Lett.* **1996**, *77*, 3865−3868.

(30) Perdew, J. P.; Chevary, J. A.; Vosko, S. H.; Jackson, K. A.; Pederson, M. R.; Singh, D. J.; Fiolhais, C. Atoms, Molecules, Solids, and Surfaces: Applications of the Generalized Gradient Approximation for Exchange and Correlation. *Phys. Rev. B* **1992**, *46*, 6671.

(31) Lefebvre, C.; Rubez, G.; Khartabil, H.; Boisson, J. C.; Contreras-Garcia, J.; Henon, E. Accurately Extracting the Signature of Intermolecular Interactions Present in the NCI Plot of the Reduced Density Gradient Versus Electron Density. *Phys. Chem. Chem. Phys.* **2017**, *19*, 17928−17936.

(32) Lu, T.; Chen, F. Multiwfn: a multifunctional wavefunction analyzer. *J. Comput. Chem.* **2012**, *33*, 580−592.

(33) Nakamoto, K. *Infrared and Raman Spectra of Inorganic and Complexes. US*, 1986.

(34) Seyidoglu, T.; Bohn, M. A. Effects of Four Isocyanates and Four Plasticizers on the Thermomechanical and Tensile Propertise of Hydroxyl-terminated Polybutadiene Elastomers and the Effect of Solid Particle Filling. *J. Appl. Polym. Sci.* **2021**, *10*, 50362−50385.
(35) Raftopoulos, K. N.; Jacia, M.; Aravopoulou, D.; Hebda, E.; Pielichowski, K.; Pissis, P. Poss Along the Hard Segments of Polyurethane. Phase Separation and Molecular Dynamics. *Macromolecules* **2013**, *46*, 7378−7386.
(36) Lee, I.; Bates, F. S. Synthesis, Structure, and Properties of Alternatingand Random Poly(styrene-b-butadiene) Multiblock Copolymers. *Macromolecules* **2013**, *46*, 4529−4539.
(37) Mathieu, J.; Stucki, H. Military High Explosives. *Chim. Int. J. Chem.* **2004**, *58*, 383−389.
(38) Abou-Rachid, H.; Lussier, L. S.; Ringuette, S.; Lafleur-Lambert, X.; Jaidann, M.; Brisson, J. On the Correlation Between Miscibility and Solubility Properties of Energetic Plasticizers/polymer Blends: Modeling and Simulation Studies. *Propellants, Explos., Pyrotech.* **2008**, *33*, 301−310.
(39) Santhosh, G.; Reshmi, S.; Reghunadhan, C. P. Rheokinetic Characterization of Polyurethane Formation in a Highly Filled Composite Solid Propellant. *J. Therm. Anal. Calorim.* **2020**, *140*, 213−223.
(40) Maka, H.; Spychaj, T.; Zenker, M. High Performance Epoxy Composites Cured with Ionic Liquids. *J. Ind. Eng. Chem.* **2015**, *31*, 192−198.
(41) Zhang, H. *Modern organic wave spectroscopy*. China, 2005.
(42) Krol, P. Synthesis Methods, Chemical Structures and Phase Structures of Linear Polyurethanes. Properties and Applications of linear polyurethanes in polyurethane elastomers, copolymers and ionomers. *Prog. Mater. Sci.* **2007**, *52*, 915−1015.
(43) Zheng, J. R.; Ozisik, R.; Siegel, R. W. Phase Separation and Mechanical Responses of Polyurethane Nanocomposites. *Polymer* **2006**, *47*, 7786−7794.
(44) Liu, Y. T.; Liu, L.; Liang, Y. R. Relationship Between Structure and Dynamic Mechanical Properties of Thermoplastic Polyurethane Elastomer Containing Bi-soft Segment. *J. Appl. Polym. Sci.* **2020**, *137*, 49141−49150.
(45) Schon, P.; Bagdi, K.; Molnar, K.; Markus, P.; Pukanszky, B.; Vancso, G. J. Quantitative Mapping of Elastic Moduli at the Nanoscale in Phase Separated Polyurethanes by AFM. *Eur. Polym. J.* **2011**, *47*, 692−698.

https://doi.org/10.1021/acsomega.3c00256
ACS Omega 2023, 8, 16738−16747